Degenerate time-dependent network dynamics anticipate seizures in human epileptic brain

Adrià Tauste Campo[1,2], Alessandro Principe[2], Miguel Ley[2], Rodrigo Rocamora[2,3*] and Gustavo Deco[1,4*]

1 Computational Neuroscience Group, Universitat Pompeu Fabra (UPF), Barcelona, Spain
2 Epilepsy Monitoring Unit, Department of Neurology, Hospital del Mar Medical Research (IMIM), Barcelona, Spain
3 Faculty of Health and Life Sciences, Universitat Pompeu Fabra (UPF), Barcelona, Spain
4 Institució Catalana de Recerca i Estudis Avançats (ICREA), Barcelona, Spain

[*] These authors contributed equally to this work.

Correspondence to: Adrià Tauste Campo,
Institut Hospital del Mar d'Investigacions Mèdiques
Barcelona Biomedical Research Park
C/ Dr. Aiguader, 88
08003 Barcelona
Spain

Abstract

Epileptic seizures are known to follow specific changes in brain dynamics. While some algorithms can nowadays robustly detect these changes, a clear understanding of the mechanism by which these alterations occur and generate seizures is still lacking. Here, we provide cross-validated evidence that such changes are initiated by an alteration of physiological network state dynamics. Specifically, our analysis of long intracranial EEG recordings from a group of 10 patients identifies a critical phase of a few hours in which time-dependent network states become less variable ("degenerate") and is followed by a global functional connectivity reduction before seizure onset. This critical phase is characterized by an abnormal occurrence of highly correlated network instances and is shown to particularly affect the activity of resection regions in patients with validated post-surgical outcome. Our approach characterizes pre-seizure networks dynamics as a cascade of two sequential events providing new insights into seizure prediction and control.

Epilepsy is among the most common neurological disorders with an estimated prevalence of about 1% of the world's population and almost 2% in low-income families in developed countries (CDC, 2010). Epilepsy is characterized by the seemingly random occurrence of seizures, which can greatly affect the quality of life of patients. Approximately one third of all epileptic patients are resistant to pharmacotherapy (Patrick *et al.*, 2011) and could benefit from a variety of surgical options. Among them, closed-loop neuromodulation based on an accurate prediction of seizure occurrences is a promising tool.

Over the last decades, several studies have showed that seizures are preceded by detectable changes in brain dynamics that can be measured via intracranial recordings. Although not being fully understood, these changes have been associated to the existence of a transition from interictal activity to *pre-ictal state* (Lopes da Silva 2003, Stacey *et al.*, 2011). These findings have motivated intense research on the development of seizure prediction algorithms for therapeutic use in patients with refractory epilepsy (Park *et al.*, 2011, Valderrama *et al.*, 2012, Cook *et al.*, 2013, Gadhoumi *et al.*, 2015). Although significant progress has been made to attain above-chance level performance results (Brinkmann *et al.*, 2016), there is yet a long road to turn seizure prediction into therapeutic devices. A major caveat of current seizure prediction is the lack of understanding about the neurophysiological processes associated to the emergence and maintenance of the pre-ictal state. Indeed, most studies have resorted to fully data-driven methods to discriminate the pre-ictal state with multiple signal features, which are typically patient-specific and difficult to interpret (Gadhoumi *et al.*, 2015).

Nowadays epilepsy research is gradually adopting a network approach to study seizure dynamics at a global level and assess the contribution of the epileptogenic zone (Van Diessen *et al.* 2013, Van Mierlo *et al.*, 2014, Goodfellow *et al.*, 2016, Khambati *et al.,* 2016). In this growing field, the majority of published studies have identified specific graph-theoretical properties of functional networks during ictal and interictal periods (Kramer *et al.*, 2008, Bartolomei *et al.*, 2011, Haneef *et al.*, 2014, Stam 2014). More recently, a few groups have highlighted the critical dependence of these findings into the dynamics of brain network states (Takahashi *et al.*, 2012, Rummel *et al*. 2013, Burns *et al.*, 2014, Khambati *et al.,* 2015). However, some questions remain open. How are physiological network states dynamically altered before epileptic seizures? Can network dynamics provide a common principle of the pre-ictal state?

In the current study, we tackled these questions by analyzing time-dependent alterations in the dynamic repertoire of the functional connectivity (Hutchinson *et al.*, 2013) during long pre-seizure periods. More specifically, we hypothesized that the variability of network states measured via graph-theoretical analysis was altered before epileptic seizures. Under this hypothesis, we developed a method to study specific variability changes prior to seizures preceded by long interictal periods in 10 epileptic patients monitored with video-SEEG

(stereoencephalography) during pre-surgical diagnosis. We made use of a graph-theoretical property, the eigenvector centrality, to characterize network states (Burns *et al.*, 2014) as instances of a time-varying multivariate continuous variable, and resorted to the Gaussian entropy (Cover and Thomas, 2012) to describe their variability. A controlled analysis using time-matched periods of interictal activity from additional days revealed a consistent and sustained decrease of the variability of network states before the seizure occurred. Remarkably, in all patients this loss of variability was specifically associated to an abnormal occurrence of high-connectivity states during the pre-seizure period. We also investigated the contribution of the epileptogenic sites to the measured effect in two patients with a very good long-lasting post-operative outcome. In particular, the application of our analysis to the mapped epileptogenic sites of these seizure-free patients showed a significant and specific alteration in the resected areas of the patients' epileptic networks. Overall, our approach provides two contributions in the analysis of epileptic network dynamics. First, it characterizes the pre-ictal state as a two-stage process in which epileptic networks undergo a functional reorganization before seizure onset. Second, it develops methodological aspects that may be considered to improve seizure prediction algorithms. More broadly, the results presented here open new lines to investigate critical alterations in pathological networks by studying the time-varying nature of brain networks.

Results

We studied network dynamics prior to epileptic seizures in 10 drug-resistant patients using continuous multichannel intracranial recordings via stereoelectroencephalography (SEEG) during pre-surgical monitoring evaluation (See details in Table 1). To capture long-term changes in network dynamics, we considered patients whose first spontaneous clinical seizure occurred after at least 30 hours (average value: 71.4±19.1 hours; mean±std) of intracranial implantation. This ictal activity exhibited variable onset times over patients that were more concentrated during the 0:00-8:00 period (Fig. 1A). For every patient, we analyzed a long continuous period (average value: 10.4±1.9 hours; mean±std) of intracranial activity before the seizure occurred (pre-seizure period, Fig. 1B). We controlled for the specificity of our findings by independently analyzing time-matched periods of interictal activity from different days (control period, Fig. 1B). In this study we could include 2 patients with very good post-surgical outcome after a minimal follow-up of 3 years (Patients 1 and 3) and two patients that

presented potential perturbation factors affecting the pre-seizure period (Patients 9 and 10). More precisely, Patient 9 had been electrically stimulated 16.5 hours before the first recorded seizure and Patient 10 presented a subclinical seizure 6.1 hours before the first clinical seizure onset.

Network dynamics analysis

We tracked network state dynamics for each patient separately over each SEEG recording session. To do so, we computed functional connectivity across all recording sites (also referred to as sites, average value: 98.3±25.1 sites; mean±std) over consecutive and non-overlapping time windows of 0.6s (Fig. 1D). Networks in each window were characterized as a weighted directed graph, where electrode contacts represented the nodes and absolute-valued pairwise correlations represented their weighted edges (Fig. 1D). We then evaluated a centrality measure for each connectivity matrix to track network dynamics in a reduced and interpretable dimensionality space. Indeed, we computed the eigenvector centrality to reduce each $N \times N$ connectivity matrix to a N-dimensional vector, where N was the total number of recording sites, thus obtaining a centrality sequence for each recording site (Fig. 1D). This measure can be equivalently interpreted as the principal component of the normalized covariance matrix of the set of intracranial recordings in each window.

Our initial hypothesis was that the pre-ictal state was associated with an alteration of physiological network states. We therefore tested this hypothesis by quantifying changes in the distribution of the eigenvector centrality sequences representing these network states. In particular, we assumed that the centrality time series could be approximated by a multivariate Gaussian distribution for a sufficiently large number of samples (n>100). In principle, the second-order variability of a multivariate variable may exhibit two components: the temporal component, i.e., how the centrality of a recording site varies as a function of time, and the spatial component, i.e., how the centrality consistently varies across recording sites at given time instance. A measure that simultaneously quantifies both components is the multivariate Gaussian entropy, which monotonically depends on the product of the covariance matrix's eigenvalues (Fig. 1C). This measure corresponds to the differential entropy of multivariate normally distributed variables (Cover and Thomas, 2012), and it can be proved useful to approximate the variability of more general variables in the large-sample regime.

Network state variability identifies time-dependent alterations before seizure onset

First, we centered our analysis on the pre-seizure period and the time-matched period from the previous day (pre-seizure, control). Over both periods we computed the multivariate Gaussian entropy in consecutive and non-overlapping time windows of 200 centrality samples (120s) and normalized the measure to lie within the interval [0,1] per patient. We shall refer to this applied measure as centrality entropy in the remaining of the article. The straightforward application of the centrality entropy to both periods showed that centrality sequences were generally less entropic during the pre-seizure period (See Fig. S1) showing a gradual increase and successive decrease of this cross-period difference as seizure onset approached. In order to localize this effect in a specific and significant time segment, we grouped consecutive entropy values into intervals and made use a non-parametric test to identify the cluster of consecutive centrality entropy intervals that was significantly yielding the largest entropy decay per patient (*Materials and methods*). The results of this test are illustrated for all patients in Fig. 2A where average centrality entropy curves are plotted for the control (in blue) and pre-seizure period (in red) together with the identified significant time segment (in cyan) during the 9.5 hours preceding the seizure. In each patient, this segment highlighted intervals where the same centrality entropy reduction could not be achieved by shuffling interval-dependent entropy values across the pre-seizure and control periods ($P<0.01$, Fig S2A). Intriguingly, the identified segment was rather patient-specific exhibiting offset times that were not generally attached to the seizure onset. However, when grouping samples across patients 1-9, significant intervals turned out to be regularly distributed around the proximity of the seizure onset with the interval [-2.5, -2] being the most frequent (Fig. 2B). In particular, this distribution was statistically different ($P<0.05$, Kolmogorov Smirnov test) from a surrogate distribution obtained by randomly placing the same segments per patient in every possible location of the pre-seizure period (Fig. 2C). In addition, relevant features of the identified segment such as the onset and offset times, and the test's statistic value were not significantly correlated with the seizure onset time (Fig. S2B, C and D), which excluded a straightforward association of the observed effect with daily rhythms. Finally, the results obtained in both patients with potential perturbation factors were rather different. Interestingly, Fig. S2A quantified the cross-period difference measured in Patient 9 to be the least significant across all patients, suggesting that a previous received

electrical stimulation might have had an effect on his pre-seizure dynamics. In contrast, the occurrence of a subclinical seizure in Patient 10 did not yield a quantitatively different result. We analyzed the stability of these results using a synchronization measure (phase-locking value) over difference frequency bands and an alternative network measure (node strength, Materials and Methods). The separate application of both measures unraveled similar trends with weaker statistical effects (Figs. S3 and S4). In conclusion, our initial findings suggested that significant and sustained reductions of network state variability over a precedent-day baseline could be related to a pre-ictal state. Further, this reduction in variability was statistically mapped to a patient-specific time period per patient that will be referred to in the following as the critical phase.

As observed earlier, the critical phase was not in general attached to the seizure onset of every patient. Hence, how could the critical phase be related to the reported evidences of the pre-ictal state? To address this question, we split both recording sessions of Patients 1-9 into the critical phase, and sub-periods immediately before (pre-critical phase) and after (post/ending critical phase) the critical phase (Fig. 2C). For those patients with critical phases attached to the seizure onset (Patients 1, 6 and 8) we considered the post-critical phase to comprise the last window time samples of the critical phase. In each sub-period we evaluated the mean functional connectivity along both recording sessions. The results shown for patients with recorded pre-critical and critical phases reveal that during the critical phase of the pre-seizure period the mean connectivity exhibited an increase that was not significant over these patients (Fig. 2C, $P>0.05$, paired Wilcoxon test, $n=8$). In contrast, when comparing the critical and the post/ending-critical phases the mean connectivity decreased significantly over all patients (Fig. 2C, $P<0.01$, paired Wilcoxon test, $n=10$), which conciliates with previous characterizations of the pre-ictal state (Mormann *et al.* 2003, Le Van Quyen *et al.*, Stacey *et al*, 2011). Interestingly these variations were not present during the control period, suggesting that the global connectivity decrease was specific of the pre-seizure period and could be driven by the critical phase.

Reduced network state variability spans across spatial and temporal domains

As introduced earlier, the centrality entropy quantified the (spatio-temporal) variability of simultaneous centrality sequences in a single scalar value. Then, how was the variability reduction individually expressed along recording sites and along time samples? To answer

this question, we repeated the previous non-parametric statistical analysis (Fig. 2A) over both recording periods using the spatial and temporal versions of centrality entropy independently (*Materials and methods*). Although the results were generally reproduced along each dimension, the variability reduction was differently distributed across space and time over patients. In sum, the decrease of network state variability observed during the pre-seizure period was associated to the occurrence of more similar centrality values over time (less temporal variability), which in general exhibited more homogeneous centrality values across recording sites (less spatial variability).

Altered occurrence of high-connectivity states explains reduction of variability.

The previous results described that network states (as modelled by the eigenvector centrality measure) became more temporally redundant and more spatially homogeneous during the critical phase. In turn, the reduced spatio-temporal variability was associated to a non-significant increase of the mean connectivity across patients (Fig 2C). Yet, how was the actual interplay between network dynamics and connectivity alterations during the pre-seizure period? An initial analysis based on the time-dependent mean connectivity (averaged over all recording sites' pairs) did not reveal consistent cross-period differences over patients (Fig. S5). Then, we related the observed reduced network variability to alterations in the occurrence of certain states. In particular, were there specific time-varying states producing this effect? We here explored this question and inspected the eigenvector centrality sequences during the control and pre-seizure periods. A visual inspection on these vector sequences for every patient suggested the hypothesis that the amount of "homogeneous states" (represented as yellow strips in the plot) was larger during the pre-seizure period than in the control period. Interestingly, these homogeneous states were specifically associated with high-connectivity correlation matrices in most of the patients (Fig. 3A).

Centrality vector sequences like the one presented in Fig. 3A were observed to be recurrent over time. Then, we used a clustering algorithm to extract the 12 most representative vectors over both periods of interest and classified each centrality vector at any given time accordingly (*Materials and methods*). Consequently, the sequence of centrality vectors turned into a sequence of discrete states whose frequency over any time interval (probability) could be computed and compared across control and pre-seizure periods. Then, we formally tested

the hypothesis that the larger presence of homogeneous states during the pre-seizure period was associated to the observed reduction in network state variability in each patient. For each patient, we linearly regressed the cross-period centrality entropy difference over two independent state regressors: state probability and state heterogeneity (measured via the standard deviation across recording sites of the same state) differences (Fig. 3B). We then computed the variance explained by each regressor via its coefficient of determination (R squared). To investigate the group-level influence of every state's connectivity into these associations, states were sorted for each patient in decreasing order of connectivity (i.e., mean connectivity of its associated correlation matrix), and coefficients of determination linked to state probability (Fig. 3C, top) and state heterogeneity (Fig. 3C, bottom) differences were distributed in boxplots for each state.

Interestingly, Fig. 3C (left) shows at the group level for both regressors (state probability and state heterogeneity) that the most influential states on the reduced variability effect were those with largest connectivity associated matrices. Specifically, the effect size between the variance explained by the highest-connectivity states and the remaining ones was large in both state probability (D=1.7) and state heterogeneity (D=2.1) over all patients. Then, we computed the Spearman correlation between the highest-connectivity regressors and the centrality entropy reduction to unravel group-level correlation trends. Correlation values were of r=0.63 (P<1e-5) and r=-0.45 (P<1e-5) for state probability and heterogeneity increases respectively indicating that the reduction of network variability was mostly explained by an increase in the frequency rate and homogeneity of the highest connectivity states.

To further investigate the interplay of high-connectivity states with the pre-seizure period, we evaluated cross-period state probability and heterogeneity differences at a patient level during the critical phase identified in Fig. 2A (Fig. 3C right). First, we found that the probability of HCS was significantly different in all patients across both periods (paired t-test, P<0.01, P<0.1). In 7 out of 9 patients HCS occurred significantly more often during the critical phase while in the remaining patients (Patients 2 and 5) HCS were less frequent. Second, the homogeneity of HCS was significantly increased in most of the patients (paired t-test, P<0.01, P<0.1), except in Patient 5 were it significantly decreased, and in Patients 2 and 9 were it remained statistically equal. Although the influence of HCS into the pre-seizure period was consistent across all patients, the different trends found in some specific patients (Patients 2 and 5) suggest that this influence might be modulated by context-dependent variables. In sum, HCS were strongly contributing to make state dynamics less variable over

time by reducing the occurrence of alternate states and imposing homogeneous centrality values across recording sites.

Cross-validation analysis in additional periods

We identified network dynamics changes in the pre-seizure period that were consistently expressed with a similar trend (sustained variability reduction) across a heterogeneous cohort of patients (Table I). Critically, these time-dependent changes could be associated to a common factor in all patients, namely, an alteration of recurrent high-connectivity time instances (0.6s) across recording sites. However, was this characterization specific of the pre-seizure period? Or could be alternatively ascribed to a post-implantation effect? To shed light into these questions, we analyzed additional 121 hours of interictal activity in 6 patients from time-matched periods that were placed two days before the seizure ('pre-control' period) and a varying number (across patients, mean=3,83) of days after the seizure ('post-control' period). These new interictal data was introduced in the analysis as schematized in Fig 4A. As control experiments, we defined two additional time-matched comparisons: a comparison between the pre-control and control periods ('C1') and a comparison between the seizure and post-seizure period ('C2'). These new comparisons were then confronted with the original comparison particularized to the 6 patients. The overall analysis was made under the condition that period lengths were time-matched and balanced across comparisons for each patient. First, for every comparison, we repeated the cluster-based analysis of Fig. 2A to determine the existence of putative critical phases in other periods. While comparison C2 only yielded one patient with a significant effect, C1 revealed that entropy reductions could occur across interictal periods in 5 out of 6 patients (Fig. 4B). Nonetheless, when grouping the six patients, the sub-periods found with C1 were not followed by a post-critical decrease of functional connectivity as in the original comparison (Fig. 4C). Finally, we repeated the regression analysis of Fig. 3B in patients with significant entropy reductions of C1 (five patients) and C0 (original comparison in six patients) and represented the results along analogous lines for each comparison. Crucially, for C1 periods, the variability decrease was more weekly explained by cross-period HCS differences than in C0 periods. Indeed, the difference in the coefficient of determination of HCS across comparisons was large in state probability (D=0.5, Cohen's D) and more notably in state homogeneity (D=1.1, Cohen's D). This resulted in a lower gap between the variance explained by HCS states and the variance explained by non-HCS states in both measurements in C1 (D=0.4 and D=0.2, Cohen's D) as

compared with C0 (D=1.2 and D=1.8, Cohen's D). Although decreases in network state variability may occur across consecutive days (C1), we provided evidence that those occurring during the pre-seizure period were specifically tied to high-connectivity states alterations and a subsequent functional connectivity decrease.

Influence of the critical phase into epileptogenic sites

Importantly, network dynamic changes observed during the pre-seizure period could be associated to an altered occurrence of HCS in all patients. Yet, how this seemingly physiologic alteration could evolve into generating seizures? In particular, how was this effect manifested in those regions that were involved in seizure generation? To further relate our findings to the ictogenesis process we particularized our analysis to the clinically mapped epileptogenic sites of two patients with very good post-surgical outcome and a follow-up period of more than three years (Patients 1 and 3, *Materials and Methods*, Table 1). Both patients are seizure free (Engel 1) with Patient 3 exhibiting some residual ictal symptomatology (seizure auras). In these patients, we specifically investigated the influence of epileptogenic sites in the pre-seizure network dynamic changes. To provide a complete comparison of sites we independently analyzed seizure-onset zone sites (SOZ, brain zone involved in the initial stages of the seizure spread), resected zone sites (RZ, brain zone that rendered seizure-freeness after its resection) and the remaining sites (nEZ, non-epileptogenic sites). We note that in Patients 1 and 3 SOZ and RZ were partially overlapping regions and SOZ was not fully included in the RZ. To carry out this region-specific analysis, we first evaluated the temporal mean and standard deviation of the recording sites' centrality in the SOZ, RZ, and nEZ sites over the control and pre-seizure periods. Fig. 5A plots the time-average centrality of RZ and nEZ as a function of the remaining time to seizure onset. Interestingly, this figure illustrates in both patients that the time-average centrality of the RZ was higher than the nEZ over each period of interest and that during the critical phase (in cyan) the centrality of RZ sites was reduced at the expense of an increase in the centrality of nEZ sites. This preliminary observation suggested that regions having a distinct pathological role could be involved in the pre-ictal dynamics. However, was the level of involvement equal across the three studied regions? Fig. 5B characterizes the network dynamics of the three regions by comparing the temporal standard deviation of their recording site's centrality in SOZ (inner left), RZ (inner central) and NEZ (inner right) regions for control (blue) and

pre-seizure (red) period, inside (outer left) and outside (outer right) the critical phase. To assess cross-period differences in regions of variable size we resorted to the effect size measured by absolute-valued Cohen's D and highlighted comparisons exceeding the value of 0.5 (large effect). Using this quantification, Fig 5B shows that the largest decrease in the centrality variability (D>0.5) of Patient 1 was only localized in the RZ during the critical phase. For Patient 3, large effect sizes were found in RZ but also in nEZ during the critical phase. Outside the critical phase, cross-period differences attained lower effect sizes.

We investigated the influence of HCS on epileptogenic and non-epileptogenic sites to further describe the functional alterations occurring during the critical phase. More specifically, we compared the average connectivity per site (node strength) in the RZ, SOZ and nEZ during the presence of the HCS and the remaining states (non-HCS) in each patient for control and pre-seizure periods in the critical phase (Fig. 5C). This analysis revealed several findings. First, the strength was more homogenous across regions during HCS states (Patient 1 std=0.04, Patient 2 std=0.01) than during nHCS states (std= 0.07, 0.03). Second, in both patients cross-period differences in strength occurred more prominently during HCS (average D >1.8) than in nHCS (average D <0.7). Further, during HCS, strengths increased from control to pre-seizure periods consistently in the three studied regions while the differences were of varying sign across regions during nHCS. Finally, the region that exhibited the highest increase in strength was the resected zone for both patients (D=2.9, 2.8), followed by the non-epileptogenic sites (D=2.2, 1.4) and the seizure-onset zone (D=1.2, 0.6). Therefore, during the critical phase, the abnormal occurrence of HCS altered the intrinsic connectivity gradient between epileptogenic and non-epileptogenic regions by inducing more homogenous connectivity while boosting the connectivity of the RZ sites. In particular, this later increased connectivity resulted in RZ exhibiting less variable centrality values during the critical phase (Fig. 5B).

We finally evaluated in both patients how the functional connectivity decrease observed during the post-critical period was distributed across the strength of the three regions (Fig. S10). The results show that the decrease was largely affecting the three regions (D≥0.9) with epileptogenic sites showing a more prominent decay (average D=1.7) than non-epileptogenic sites (average D=1.35).

Discussion

This study examined the existence of a common alteration principle in brain network dynamics during long-lasting periods of activity preceding the first clinical seizure in 10 patients with focal refractory epilepsy. Using a comparative analysis between genuine pre-seizure periods and time-matched periods of intericral activity per patient, we were able to consistently show a sustained decrease in the variability of network states that was followed in most of the patients by a functional connectivity drop of approximately 30 minutes before the seizure onset (Fig. 6). Further analysis revealed factors altering this variability in the temporal (time samples) and spatial (recording sites) domains. First, this decrease in network variability was associated with an abnormal occurrence of high-connectivity states during pre-seizure periods as compared to previous days. Second, the reduction in temporal variability was mainly localized in the resected zone of two patients with best post-surgical outcome.

The work presented here makes use of a novel approach to quantify the network dynamics alterations that occur during the pre-ictal period. Over the last decade, fMRI studies have showed growing evidence that dynamic connectivity patterns ("brain dynamic repertoire") may be an intrinsic property of brain function and disease (Hutchinson *et al.*, 2013). Particular examples of disrupted dynamics have been found in Alzheimer's disease (Jones *et al.*, 2012) and neuropsychiatric disorders (Damaraju *et al.*, 2014) whose translation to new clinical biomarkers is currently matter of discussion (Deco and Krigelback 2014, and references therein). In modern epilepsy research, the dynamic principle of brain function has been postulated to be commonplace to understand the ictogenesis process (Richardson 2012) but most network studies have studied alterations in static functional networks with a few exceptions (Dimitriadis *et al*., 2012, Morgan *et al.,* 2015).

When studying the variability of brain dynamics along long recording periods, one is confronted with the confounding effect of circadian rhythms (Kuhnert *et al.*, 2010, Rocamora *et al.*, 2013, Geier *et al.*, 2015), which span across sleep and wake phases. These rhythms may become critical when one characterizes specific brain configurations associated with the pre-ictal state, which has been shown to approximately last 4 hours (Mormann *et al.*, 2007).

Previous studies on the pre-ictal state have analyzed pre-ictal changes with reference to previous interictal periods, not necessarily time-matched. Inspired by a previous work (Andrzejak *et al.*, 2003), the strategy used here tackled this issue by defining time-matched reference periods from precedent and subsequent days, thus allowing for a more specific identification of pre-ictal changes in brain network dynamics. Nonetheless, the existence of time-locked brain dynamics at the scale of tenths of minutes is an assumption that may not suffice to control for all physiological phase transitions. Hence, whether altered network dynamics were produced by time shifts in sleep/awake phase transitions across both days or a change within a single sleep/wake phase was not fully addressed in this study. Yet, our preliminary results on the relationship between patient's putative critical phases and seizure onset times do not seem to support the phase time-shift hypothesis. In any event, a larger cohort of patients with variable seizure times and a good readout of their sleep phases will be necessary to address this question in the future. Another key aspect of the study is the use of the first monitored clinical seizure occurring during the first implantation days. This choice was pivotal to analyze comparable long-term network dynamic changes across patients with limited influence of confounding factors such as the reduction of antiepileptic drugs, the effect of previous ictal processes and the response to clinical stimulation. In most of the studied patients this first seizure was the first event of a succession of seizures separated by short interictal periods of a few hours, which are clinically known as seizure clusters (Rose *et al.*, 2003). Hence, understanding the pre-ictal process of this initial seizure can also have important consequences for the control of later correlated events. In any event, the network analysis introduced here should be extended to subsequent seizures in future studies to determine whether the presented characterization is specific of seizures preceded by long interictal periods.

A central question in seizure prediction research has been the role of synchronization (Jiruska *et al.*, 2013) during the pre-ictal period. Some studies have reported drops in synchronization a few hours before seizure onset (Mormann *et al.*, 2003) while others have pinpointed the coexistence of distinct synchronization states depending on the recorded structures (Le Van Quyen *et al.*, 2005, Van Mierlo *et al.*, 2014). Even though a clear mechanism of such alterations is still missing, the most successful algorithms applied to large data sets make use of correlation matrices as key data features (Binkmann *et al.*, 2016). The findings presented in this study support the view that pre-ictal correlation patterns are state dependent and hence,

their alterations should be interpreted according to underlying state dynamics (Le Van Qyuen *et al.*, 2005, Takahashi *et al.*, 2012). More precisely, our results suggest that a time-dependent variation in the occurrence of highly correlated time instances may be at the origin of the pre-ictal state. This variation was manifested in most of the patient a an excess of high-connectivity states, while in two patients it was manifested as a deficit. Although pre-ictal connectivity trends are known to be patient-specific (Jiruska *et al.*, 2013), they should be further investigated against the influence of controlled behavioural states, a question that was out of the scope of this study.

Over recent years there is accumulated evidence that seizure generation and spread involves complex interactions between seizure-generating and surrounding areas (Rummel *et al.* 2013, Khambati *et al.,* 2015, Khambati *et al.,* 2016). Evaluating network dynamics in patients with good post-surgical outcome, we were able to relate our findings to clinically mapped epileptogenic sites, namely the seizure onset zone and the resected zone, as well as the remaining sites. In these patients the average contacts' centrality was higher in the epileptogenic sites for the entire analyzed periods in line with previous studies (Wilke *et al.*, 2011, Van Mierlo *et al.*, 2013). Not surprisingly, changes in this average centrality level across periods occurred during the critical phase where centrality values from both regions approached (Fig. 5A). Crucially, this change in the time-average centrality was accompanied by a significant decrease in the centrality (temporal) variability of the resected zone (Fig. 5B), which was specific in Patient 1 and also present in the non-epileptogenic sites in Patient 3 who presented a slightly worse post-surgical outcome. The analysis on the influence of high-connectivity states into validated epileptogenic sites provided initial evidence that these states might destabilize the epileptic network by reducing the connectivity gradient between epileptogenic and non-epileptogenic sites and increasing the connectivity of critical parts of the network (resected zone) during the critical phase (Fig. 5C). As a result, high-connectivity states induce the coordination of key nodes of the epileptic network and surrounding areas before seizure onset in line with previous studies (Khambati *et al.,* 2016). The consequence of this phase is shown to be a global functional connectivity decrease, which is more prominently manifested across specific epileptic nodes (Fig. S10). We speculate that this decrease in connectivity could be the result of critical sites of the epileptic network adopting a more autonomous activity that would result in the generation of a seizure. Yet, a larger study including more seizure-free patients will be necessary to fully elucidate the mutual

influence of physiological network dynamics and the epileptic network during the transition from interictal activity to focal seizures.

The results shown in this study prompt to further investigate the exact physiological origin of the reported network alterations considering putative factors like sleep deprivation or antiepileptic drugs reduction. Some considerations are yet to be mentioned. First, the use of intracranial recordings is a limiting factor in the spatial analysis of brain states, thus making them a priori subject-dependent. Nonetheless, it is recognized that the SEEG methodology offers an optimal temporal and spatial resolution of neurophysiological recordings for neural signal analysis in comparison with other techniques in patients with epilepsy. Second, the definition of network states was based on the principal component of linear correlation matrices computed in signals' broadband spectrum. Although this approach was convenient to interpret the obtained results, we expect that the overall analysis could benefit from considering non-linear coupling measures applied at specific frequency bands. In conclusion, this work provides electrophysiological evidence for characterizing the pre-seizure period as a long-lasting process in which epileptic networks undergo a sequential functional reorganization. Further investigations under this conception will help unravel seizure generation mechanisms from a network perspective, provide practical insights into how to predict and control ictal activity, and may constitute a general approach to analyze dynamic alterations of other neuropathologies.

Materials and Methods

Patients and recordings

A total number of 324 hours of SEEG recordings from ten patients with pharmacoresistant focal-onset seizures were analyzed. A summary of the patients' characteristics is given in Table 1. We included patients who presented the first seizure in a time frame that allowed us to perform a controlled analysis of EEG recordings during the pre-seizure period. Specifically, each patient in the study was selected if her first video-SEEG monitored clinical seizure had occurred after at least 30 hours (average value: 71.4±19.1 hours; mean±std) with no presence of spontaneous clinical seizures. Among the selected patients we included two patients presenting potential perturbation factors affecting the pre-seizure period (Patients 9

and 10). Patient 9 had been electrically stimulated 16.5 hours before the first recorded seizure and Patient 10 presented a subclinical seizure 6.1 hours before the first clinical seizure onset.

For each patient, the selection of recording sessions was as follows. We considered up to 12 hours before the first monitored clinical seizure occurred. As a baseline reference, we selected the same time period from the previous day (control period). For independent validation of our results, we selected additional time-matched periods of variable length in 6 patients (Patients 2-6 and 8, average period length: 10 hours) from two days before the seizure onset (pre-control period), and a few days after the seizure onset (post-control period, average value=3.83 days). No more patients could be added to the validation analysis for pre-ictal time limitations (Patients 7 and 10), a substantial modification on the implantation montage during the first monitoring days (Patient 1) or the presence of direct electrical stimulation sessions in the iEEG (Patient 9).

After detecting recording cuts in a few patients, we restricted the analysis to 11 hours per session in patients 1-9 and to 2.4 hours per recording session in Patient 10 to ensure a time-matched cross-period comparison. Among the selected patients, two patients achieved seizure freedom after surgical resection and radiofrequency thermocoagulation (RFTC, Cossu *et al.* 2015) with a follow-up of 3 years and 2 years respectively (Patients 1 and 2, Engel 1A). An additional patient only exhibited seizure auras after surgical resection and a follow-up of 3 years (Patient 3, Engel 1B). We considered Patients 1 and 3 to have a validated very good post-surgical outcome. Hence, for the purpose of analyzing epileptogenic sites, we separately considered the diagnosed seizure onset zone and the resected zone of these two patients. The seizure-onset zone was independently marked by two epileptologists (AP and RR) and consisted of n=5 (anterior hippocampus) and n=9 (anterior hippocampus, amygdala) recording sites for Patient 1 and 3 respectively. The resected zone covered 24 contacts in Patient 1 (parts of anterior hippocampus, temporal pole and entorhinal cortex) and 12 contacts in Patient 3 (parts of anterior, posterior hippocampus, and amygdala). The remaining patients were not considered in this analysis because they presented one of these cases: they had not undergone surgery (Patients 2, 6, 8, 9), had a non-sufficiently long follow-up period (<6 months, Patients 4 and 5), had not been yet operated (Patient 7) or exhibited a bad post-operative outcome (Patients 10).

All recordings were performed using a standard clinical EEG system (XLTEK, subsidiary of Natus Medical) with a 500 Hz sampling rate. A uni- or bilateral implantation was performed accordingly, using 5 to 15 intracerebral electrodes (Dixi Médical, Besançon, France; diameter: 0.8 mm; 5 to 15 contacts, 2 mm long, 1.5 mm apart) that were stereotactically inserted using robotic guidance (ROSA, Medtech Surgical, Inc).

Data pre-processing

EEG signals were processed in the referential recording configuration (i.e., each signal was referred to a common reference). The sets of electrodes included in this analysis are reported in Table 1 and displayed in Fig. 1 (top row). All recordings were filtered to remove the effect of the alternate current (Notch at 50 Hz and harmonics using a FIR filter). Then signals were further band-pass filtered between 1Hz and 150 Hz to remove slow drifts and aliasing effects respectively. Artifacts were removed in each period by detecting time window samples 600ms) where mean correlation values and recording site average signal amplitudes were 3 standard deviations larger than their median values across each period.

To perform functional connectivity analysis each EEG signal was divided into consecutive and non-overlapping 0.6s-long windows (300 samples with 500Hz sampling rate) to balance the requirements of approximate stationarity of the time series (requiring short epochs) and of sufficient data to allow accurate correlation estimates (requiring long epochs).

Functional connectivity analysis

There are different methods to assess functional connectivity from time series data based on coupling measures (Pereda *et al.*, 2005, Wendling *et al.*, 2009). Previous research on the comparison of linear and non-linear coupling measures has resulted in having distinct "ideal" measures for distinct studied situations (Stefan *et al.*, 2013). Here we chose to employ a zero-lagged linear correlation measure for its good tradeoff between simplicity and robustness (Wendling *et al.*, 2009) and more importantly, because it allowed for a convenient definition of *network state* as it will be explained later.

Leat x and y be two N-length time series representing two recorded signals during 0.6-s long epoch and let $\bar{x}$ and $\bar{y}$ be their respective sample means. Their sample (Pearson) is estimated as

$$r(x,y) \triangleq \frac{\sum_{i=1}^{N}(x(i)-\bar{x})(y(i)-\bar{y})}{\sqrt{\sum_{i=1}^{N}(x(i)-\bar{x})^2}\sqrt{\sum_{i=1}^{N}(y(i)-\bar{y})^2}} \quad . \tag{1}$$

For each patient and each consecutive 0.6s-long window we computed the absolute value of the coupling measure across all pairs of electrode contacts. For most of the patients, the overall pairwise computations resulted in approximately 123000 sequential connectivity matrices combining both recording sessions (control and pre-seizure periods). In the current study, we did not test the statistical significance of each pairwise coupling since our purpose was to track the overall network dynamics regardless of pairwise thresholding methods.

Definition of network states

For each patient, we characterized each correlation matrix as a functional network. This network was modelled as a weighted undirected graph, where electrode contacts represented the nodes and pairwise correlation values across represented their weighted edges (Ponten *et al.*, 2007). Then, we computed the network measure of eigenvector centrality for each connectivity matrix (Newman, 2010). For a given graph $G=(V,E)$, let $A=(a_{v,t})$ be its weighted adjacency matrix. The relative centrality score x_v of vertex v can be defined as

$$x_v = \frac{1}{\lambda}\sum_{t\in V} a_{v,t}x_t \quad , \tag{2}$$

which can be rearranged in a matrix form as $\lambda\ x = Ax$.

Given the requirement that all entries in x must be non-negative, the Perron-Frobenius theorem implies that only the greatest eigenvalue results in a proper centrality measure (Newman 2010). Hence, the centrality measure is given by the eigenvector associated with the largest eigenvalue of the connectivity matrix. Then, the ith contact is assigned the ith component of this eigenvector where i goes from 1 to number of recording sites in a patient. The eigenvector centrality is by definition a self-referential measure of centrality, i.e., nodes

have high eigenvector centrality if they connect to other nodes that have high eigenvector centrality (Rubinov and Sporns, 2010), which ultimately provides a measure of relative importance of each node in the network. The eigenvector centrality measure has been applied to resting-state fMRI studies (Lohmann *et al.*, 2010) and more recently to ECoG recordings of epileptic patients (Burns *et al.*, 2014).

By computing the centrality in each 0.6s-long connectivity matrix we obtained for each patient independent eigenvector centrality sequences along each recording session. If we consider each connectivity matrix to represent a brain state (Allen *et al.*, 2014), these vectors can be regarded as representative elements of these states in a vector space of dimension equal to the number of recording sites. Further, these vectors point to the direction that best summarizes the original brain state. In particular, every time that a significant change arises in the connectivity matrix, the eigenvector centrality rotates to update the relative importance ("centrality") of each contact within the new network configuration.

Choice of zero-lag correlation and eigenvector centrality

Computing the eigenvector centrality over zero-lag connectivity matrices was key to regard our network state measure as an informative summary of how the set of iEEG recording were instantaneously coupled at a given short time window. Indeed, under these conditions, the eigenvector centrality corresponds by definition to the first principal component of the (normalized) covariance matrix, i.e., the vector in the space of recording sites that accounts for the largest variance of the whole set of (normalized) iEEG recordings in a given time window.

Combinations of other coupling measures and network features could led to alternative definitions of network states. For the sake of comparison, we also provide in the Supplementary Information the results obtained by combining zero-lagged correlation with a different network feature, the node strength, which can be defined as the average pairwise connectivity of this node with the remaining ones (Rubinov and Sporns 2010, Khambhati *et al.*, 2016). Fig. S3 shows that the node strength yielded in general statistically weaker results than the eigenvector centrality. Further, we investigated the possibility of combining a synchronization measure such as the phase-locking value (Lachaux *et al.*, 1999) with the eigenvector centrality. This measure may capture contributions of non-zero lag couplings as

well as non-linear effects. To illustrate the difference between both measures in the frequency domain, we repeated the cluster-based statistical analysis of Fig. 2A for consecutive frequency narrow bands of 4Hz (from 1 to 120). Fig. S4 shows that the results were qualitatively similar across all bands for most of the patients. Yet, in those patients where discrepancies were found, the phase-locking value measure yielded weaker peaks than the zero-lag correlation.

Evaluating network state dynamics via Gaussian entropy

Our goal was to evaluate the variability of these representative states in each period. The long sequence of centrality vectors for each period can be equivalently regarded as a stream of simultaneous centrality time series, one for each recorded contact. Then, one can evaluate the spatio-temporal variability of the centrality time series through the application of the multivariate Gaussian entropy (Cover and Thomas, 2012) in a given estimation time window that we choose for this study to be 120s. The multivariate Gaussian entropy is defined as

$$H_c = \frac{k}{2}\left(1 + \ln(2\pi)\right) + \frac{1}{2}\ln\det(\Sigma), \tag{3}$$

where k is the number of recording sites, and ∑ is the covariance matrix of the centrality time series estimated in a the estimation windows. By considering centrality vectors to be independent, ∑ in (4) becomes a diagonal matrix, and the Gaussian entropy captures the aggregated variability of the centrality vectors across the temporal dimension:

$$H_c^{(1)} = \frac{k}{2}\left(1 + \ln(2\pi)\right) + \frac{1}{2}\sum_{i=1:k}\ln\Sigma_{i,i}. \tag{4}$$

By subtracting (5) from (4), one can evaluate the variability of the centrality vectors across the spatial dimension:

$$H_c^{(2)} = \frac{1}{2}\left(\ln\det\Sigma - \sum_{i=1:k}\ln\Sigma_{i,i}\right). \tag{5}$$

Hence, the two contributions sum up to give the Gaussian entropy (4):

$$H_{\mathrm{c}} = H_{\mathrm{c}}^{(1)} + H_{\mathrm{c}}^{(2)}. \tag{6}$$

State clusterization

To associate the network variability decreased observed in all patients with the occurrence of specific recurrent connectivity states, we jointly clustered the eigenvector centrality sequences in any time-matched period comparison using the k-means algorithm (Forgy, 1965). We applied this clusterization in patients 1-9 where the number of eigenvector centrality samples was comparable. In the main results we fixed the number of clusters to 12 to cover a sufficiently wide range of visually inspected connectivity states per patient. This cluster size was selected after exploring the stability of the results illustrated in Fig. 4 for the range of values n=8:12. In particular, Fig. S9 shows that these results were qualitatively very similar for the choices n=8,10,12.

Statistical analysis

The pre-seizure decrease in centrality entropy was statistically tested as follows. We started by windowing consecutive entropy samples (n=15, 30 minutes) in non-overlapping and paired time segments across each period and then we computed the effect size for each segment pair using Cohen's D (Cohen's D, Cohen, 1992). We then clustered adjacent segments with a criterion of effect size being larger of 0.15 (low-medium effect, Cohen, 1992) over a minimum of 4 adjacent segments (2 hours), and considered the aggregated sum of these segments' effect sizes as the main statistic. We further checked the statistical significance of this value through non-parametric statistical testing based on Monte Carlo sampling (Maris and Oostenveld, 2007). More concretely, for each patient with time segments satisfying the above criterion, we computed 1,000 random permutations of the centrality entropy samples across both conditions (within pre-seizure or control period) at each time segment, and repeated the same segment clusterization procedure to obtain 1000 surrogate statistic values. These values were used to approximate a null distribution against which we compared the original aggregated effect size value via a right-tail sided significance test. If the test's significance value was below 0.05, we considered the pre-seizure interval formed by the adjacent segments to exhibit significantly lower centrality entropy than the one obtained in the control period and we identified it as a *critical phase*. In addition, we made use of the Kolmogorov Smirnov test to assess that the critical phase distribution across patients was significantly different from a distribution of randomly placed significant clusters of the same duration.

In general, to test differences across time (pre-seizure vs. control period) or recording sites (seizure-onset sites resected sites, non-epileptogenic sites) per patient, we made use of the effect size based on Cohen's D for small and non-comparable number of samples, the paired Wilcoxon test for small sample sizes, the paired t-test for sufficiently large number of samples. We resorted to linear regression and the coefficient of determination to evaluate the association of state probabilities and state homogeneities with respect to the decrease in centrality entropy. Finally, mean connectivity values across electrode pairs were computed using the Fisher transform (Fisher, 1920).

Note on the tipology of statistical tests

The main results combined within-subject and group-level statistical tests depending on the the question at hand. Within-subject tests can be found in Fig. 2A, Fig. 3C right and Fig 5. Group-level tests can be found in Figs. 2B and 2C, Fig. 3C left, and Fig. 4.

Acknowledgements

We would like to thank Dr. Ralph Andrzejak, Dr. Maria Victoria Puig and Dr. Thomas Gener for their insightful comments during the preparation of this manuscript.

Funding

G.D. was supported by the European Research Council Advanced Grant DYSTRUCTURE (Grant 295129) and by the Spanish Research Project SAF2010-16085. A.T.C. was supported by the European Community's Seventh Framework Programme (FP7/2007-2013) under Grant Agreement PEOPLE- 2012-IEF-329837.

Author contributions

A.T.C. and A.P. acquired the data; A.T.C. analysed the data and wrote the manuscript. All authors contributed to the design of the study paradigm and the interpretation of the results.

Competing financial interests

The authors declare no competing financial interests.

References

Andrzejak RG, Mormann F, Kreuz T, Rieke C, Kraskov A, Elger CE, Lehnertz K. Testing the null hypothesis of the nonexistence of a preseizure state. *Physical Review. E, Statistical, Nonlinear, and Soft Matter Physics.* 2013;67(1 Pt 1), 10.1103/PhysRevE.67.010901

Allen EA, Damaraju E, Plis SM, Erhardt EB, Eichele T, Calhoun VD. Tracking whole-brain connectivity dynamics in the resting state. *Cereb Cortex*. 2014;24(3):663-676. 10.1093/cercor/bhs352

Bartolomei F, Gavaret M, Hewett R, Valton L, Aubert S, Regis J, Wendling F, Chauvel P. Neural networks underlying parietal lobe seizures: A quantified study from intracerebral recordings. *Epilepsy Res*. 2011;93(2-3):164-176. 10.1016/j.eplepsyres.2010.12.005

Brinkmann BH, Wagenaar J, Abbot D, Adkins P, Bosshard SC, Chen M, Tieng QM, He J, Muñoz-Almaraz FJ, Botella-Rocamora P, Pardo J, Zamora-Martinez F, Hills M, Wu W, Korshunova I, Cukierski W, Vite C, Patterson EE, Litt B, Worrell GA. Crowdsourcing reproducible seizure forecasting in human and canine epilepsy. *Brain*. 2016;139(6), 1713-1722. 10.3102/0002831212437854

Burns SP, Santaniello S, Yaffe RB, Jouny CC, Crone NE,Anderson WS, Sarma SV.. Network dynamics of the brain and influence of the epileptic seizure onset zone. Proc Natl Acad Sci 2014; 111: 5321-30. 10.1073/pnas.1401752111

Centers for Disease Control and Prevention (CDC) "Epilepsy in adults and access to care--United States, 2010." MMWR. Morbidity and mortality weekly report 2012 61.45: 909.

Cohen J. A power primer. *Psychol Bull*. 1992;112(1):155-159.

Cook MJ, O'Brien TJ, Berkovic SF, Murphy M, Morokoff A, Fabinyi G, D'Souza W, Yerra R, Archer J, Litewka L, Hosking S, Lightfoot P, Ruedebusch V, Sheffield WD, Snyder D, Leyde K, Himes D. Prediction of seizure likelihood with a long-term, implanted seizure advisory system in patients with drug-resistant epilepsy: A first-in-man study. *Lancet Neurol*. 2013;12(6):563-571. 10.1016/S1474-4422(13)70075-9

Cossu M, Fuschillo D, Casaceli G, Pelliccia V, Castana L, Mai R, Francione S, Sartori I, Gozzo F, Nobili L, Tassi L, Cardinale F, Lo Russo G. Stereoelectroencephalography-guided radiofrequency thermocoagulation in the epileptogenic zone: a retrospective study on 89 cases. *J Neurosurg*. 2015; 1-10.

Cover TM, Thomas JA. *Elements of information theory*. John Wiley & Sons, 2012.

Damaraju E, Allen EA, Belger A, Ford JM, McEwen S, Mathalon DH, Mueller BA, Pearlson GD, Potkin SG, Preda A, Turner JA, Vaidya JG, van Erp TG, Calhoun VD. Dynamic functional connectivity analysis reveals transient states of dysconnectivity in schizophrenia. *NeuroImage: Clinical*. 2014. *5*(July), 298–308. 10.1016/j.nicl.2014.07.003

David O, Blauwblomme T, Job AS, Chabardès S, Hoffmann D, Minotti L, Kahane P. Imaging the seizure onset zone with stereo-electroencephalography. *Brain.* 2011; 134(Pt 10): 2898-911.

Deco G, Kringelbach ML. Great expectations: Using whole-brain computational connectomics for understanding neuropsychiatric disorders. *Neuron*. 2014. 84(5), 892–905. http://doi.org/10.1016/j.neuron.2014.08.034

De Curtis M, Gnatkovsky. Reevaluating the mechanisms of focal ictogenesis: the role of low-voltage fast activity. Epilepsia,. 2009. 50(12), 2514-2525.

Dimitriadis SI, Laskaris NA, Del Rio-Portilla Y, Koudounis GC. Characterizing dynamic functional connectivity across sleep stages from EEG. *Brain Topography*. 2009;*22*(2), 119–133. 10.1007/s10548-008-0071-4

Draguhn A, Traub RD, Schmitz D, Jefferys JGR. Electrical coupling underlies high-frequency oscillations in the hippocampus in vitro. *Nature.* 1998; 394: 189-192.

Fischl B. FreeSurfer. *Neuroimage* 2012; 62:774-81.

Fisher RA. Frequency distribution of the values of the correlation coefficient in samples from an indefinitely large population. *Biometrika*.1914, 10(4), 507-521.

Forgy EW. Cluster analysis of multivariate data: efficiency versus interpretability of classifications. *Biometrics.* 1965; 21: 768-69.

Gadhoumi K, Lina JM, Mormann F, Gotman J. Seizure prediction for therapeutic devices: A review. *J Neurosci Methods*. 2015;(029):1-13. 10.1016/j.jneumeth.2015.06.010

Geier C, Lehnertz K, Bialonski S. Time-dependent degree-degree correlations in epileptic brain networks: from assortative to dissortative mixing. *Frontiers in Human Neuroscience*, *9*(August), 462. 10.3389/fnhum.2015.00462

Goodfellow M, Rummel C, Abela E, Richardson MP, Schindler K, Terry JR. Estimation of brain network ictogenicity predicts outcome from epilepsy surgery. *Scientific Reports*. 2016;6:1-13.

Hudetz AG, Liu X, Pillay S. Dynamic Repertoire of Intrinsic Brain States Is Reduced in Propofol-Induced Unconsciousness. *Brain Connect*. 2015;5(1):10-22.

Hutchison RM, Womelsdorf T, Allen EA, Bandettini PA, Calhoun VD, Corbetta M, Della Penna S, Duyn JH, Glover GH, Gonzalez-Castillo J, Handwerker DA, Keilholz S, Kiviniemi V, Leopold DA, de Pasquale F, Sporns O, Walter M, Chang C. Dynamic functional connectivity: Promise, issues, and interpretations. *Neuroimage*. 2013;80:360-378.

Jiruska P, de Curtis M, Jefferys JGR, Schevon CA, Schiff SJ, Schindler K. Synchronization and desynchronization in epilepsy: controversies and hypotheses. *J Physiol*. 2013;591(4):787-797. 10.1113/jphysiol.2012.239590

Khambhati AN, Davis KA, Oommen BS, Chen SH, Lucas TH, Litt B, Bassett DS. Dynamic network drivers of seizure generation, propagation and termination in human neocortical epilepsy. *PLoS Comput Biol*. 2015;11(12) 1-19. 10.1371/journal.pcbi.1004608

Khambhati AN, Davis KA, Lucas TH, Litt B, Bassett DS. Virtual cortical resection reveals push-pull network control preceding seizure evolution. *Neuron*. 2016:91(5), 1170-1182.

Kramer MA, Kolaczyk ED, Kirsch HE. Emergent network topology at seizure onset in humans. *Epilepsy Research*. 2008;*79*(2-3), 173–186. 10.1016/j.eplepsyres.2008.02.002

Kramer MA, Eden UT, Lepage KQ, Kolaczyk ED, Bianchi MT, Cash SS. Emergence of persistent networks in long-term intracranial EEG recordings. *J Neurosci 2011*; 31:15757-67.

Kerr MS, Burns SP, Gale J, Gonzalez-Martinez J, Bulacio J, Sarma SV. Multivariate analysis of SEEG signals during seizure. In *2011 Ann Int Conf IEEE Eng Med Biol Soc.* 2011; 8279-82.

Kuhnert MT, Elger CE, Lehnertz K. Long-term variability of global statistical properties of epileptic brain networks. *Chaos 20*(2010),043126. 10.1063/1.3504998

Jones DT, Vemuri P, Murphy MC, Gunter JL, Senjem ML, Machulda MM, Przybelski SA, Gregg BE, Kantarci K, Knopman DS, Boeve BF, Petersen RC, Jack CR Jr. Non-stationarity in the "resting brain's" modular architecture. *PLoS ONE*. 2012;*7*(6).

Lachaux JP, Rodriguez E, Martinerie J,Varela FJ. Measuring phase synchrony in brain signals. *Hum Brain Mapp.* 1999;8(4):194-208.

Le Van Quyen M, Soss J, Navarro V, Robertson R, Chavez M, Baulac M, Martinerie J. Preictal state identification by synchronization changes in long-term intracranial EEG recordings. *Clin Neurophysiol*. 2005;116(3):559-568. 10.1016/j.clinph.2004.10.014

Liao W, Zhang Z, Mantini D, Xu Q, Ji GJ, Zhang H, Wang J, Wang Z, Chen G, Tian L, Jiao Q, Zang YF, Lu G. Dynamical intrinsic functional architecture of the brain during absence seizures. *Brain Struct Funct*. 2014;219(6):2001-2015. 10.1007/s00429-013-0619-2

Lohmann G, Margulies DS, Horstmann A, Pleger B, Lepsien J, Goldhahn D, Schloegl H, Stumvoll M, Villringer A, Turner R. Eigenvector centrality mapping for analyzing connectivity patterns in fMRI data of the human brain. *PLoS One*. 2010;5(4). 10.1371/journal.pone.0010232

Lopes da Silva F, Blanes W, Kalitzin SN, Parra J, Suffczynski P, Velis DN. Epilepsies as dynamical diseases of brain systems: basic models of the transition between normal and epileptic activity. *Epilepsia.* 2003;44 (Suppl 12): 72–83.

Maris E, Oostenveld R. Nonparametric statistical testing of EEG- and MEG-data. *J Neurosci Methods*. 2007;164(1):177-190. 10.1016/j.jneumeth.2007.03.024

Mirowski P, Madhavan D, LeCun Y, Kuzniecky R. Classification of patterns of EEG synchronization for seizure prediction. *Clin Neurophysiol.* 2009; 120: 1927-40.

Morgan VL, Abou-Khalil B, Rogers BP. Evolution of Functional Connectivity of Brain Networks and Their Dynamic Interaction in Temporal Lobe Epilepsy. *Brain Connectivity.* 2014;*5*(1):35–44.

Mormann F, Kreuz T, Andrzejak RG, David P, Lehnertz K, Elger CE. Epileptic seizures are preceded by a decrease in synchronization. *Epilepsy Research*. 2013;*53*(3), 173–185. 10.1016/S0920-1211(03)00002-0

Mormann F, Andrzejak RG, Elger CE, Lehnertz K. Seizure prediction: the long and winding road. *Brain.* 2007; 130 (Pt 2): 314-33. 10.1093/brain/awl241

Newman MEJ. Networks: An introduction. Oxford University Press; 2010. 10.1057/9780230226203.1064

Park Y, Luo L, Parhi KK, Netoff T. Seizure prediction with spectral power of EEG using cost-sensitive support vector machines. *Epilepsia*. 2011;52(10):1761-1770. 10.1111/j.1528-1167.2011.03138.x

Patrick K, Schachter SC, Brodie MJ. Drug-resistant epilepsy. N Engl J Med 2011; 365: 919-26.

Pereda E, Quiroga RQ, Bhattacharya J. Nonlinear multivariate analysis of neurophysiological signals. *Prog Neurobiol* 2005; 77:1-37.

Ponten SC, Bartolomei F, Stam, CJ. Small-world networks and epilepsy: graph theoretical analysis of intracerebrally recorded mesial temporal lobe seizures. *Clin Neurophysiol.* 2007;118:918-27. 10.1016/j.clinph.2006.12.002

Richardson MP. Large scale brain models of epilepsy: dynamics meets connectomics. *J Neurol Neurosurg Psychiatry*. 2012;83(12):1238-1248. 10.1136/jnnp-2011-301944

Rocamora R, Andrzejak RG, Jimenez-Conde J, Elger CE. Sleep modulation of epileptic activity in mesial and neocortical temporal lobe epilepsy: A study with depth and subdural electrodes. Epilepsy and Behavior 2013; 28 (2):185-190.

Rose AB1, McCabe PH, Gilliam FG, Smith BJ, Boggs JG, Ficker DM, Moore JL, Passaro EA, Bazil CW; Consortium for Research in Epilepsy. Occurrence of seizure clusters and status epilepticus during inpatient video-EEG monitoring. Neurology 2003; 60(6):975-8.

Rubinov M, Sporns O. Complex network measures of brain connectivity: uses and interpretations. Neuroimage 2010; 52: 1059-69.

Rummel C, Goodfellow M, Gast H, Hauf M, Amor F, Stibal A, Mariani L, Wiest R, Schindler K. A systems-level approach to human epileptic seizures. *Neuroinformatics*. 2013;11(2), 159-173. 10.1007/s12021-012-9161-2

Santaniello S, Sherman DL, Thakor NV, Eskandar EN, Sarma SV. Optimal control based Bayesian detection of clinical and behavioral state transitions. IEEE Trans Neural Syst Rehabil Eng 2012; 20: 708–19.

Stacey W, Le Van Quyen M, Mormann F, Schulze-Bonhage A. What is the present-day EEG evidence for preictal state? *Epilepsy Res*. 2011;97(3):243-251. 10.1016/j.eplepsyres.2011.07.012

Stam CJ. Modern network science of neurological disorders. *Nat Rev Neurosci.* 2014;15:683-95. 10.1038/nrn3801

Stefan H, da Silva FHL. Epileptic neuronal networks: methods of identification and clinical relevance. *Front Neurol.* 2013; 4.

Takahashi H, Takahashi S, Kanzaki R, Kawai K. State-dependent precursors of seizures in correlation-based functional networks of electrocorticograms of patients with temporal lobe epilepsy. *Neurol Sci.* 2012;33:1355-64. 10.1007/s10072-012-0949-5

Tagliazucchi E, Carhart-Harris R, Leech R, Nutt D, Chialvo DR. Enhanced repertoire of brain dynamical states during the psychedelic experience. *Hum Brain Mapp*. 2014;35(11):5442-5456. 10.1002/hbm.22562

Valderrama MC, Alvarado C, Nikolopoulos S, Martinerie J, Adam C, Navarro V, Le Van Quyen M. Identifying an increased risk of epileptic seizures using a multi-feature EEG–ECG classification. *Biomed Sig Proc and Control.* 2012;7:237-44.

Van Diessen E, Diederen SJH, Braun KPJ, Jansen FE, Stam CJ. Functional and structural brain networks in epilepsy: What have we learned? *Epilepsia*. 2013;54(11):1855-1865. 10.1111/epi.12350

Van Mierlo P, Carrette E, Hallez H, Raedt R, Meurs A, Vandenberghe S, Van Roost D, Boon P, Staelens S, Vonck K. Ictal-onset localization through connectivity analysis of intracranial EEG signals in patients with refractory epilepsy. *Epilepsia*. 2013;54(8):1409-1418.

van Mierlo P, Papadopoulou M, Carrette E, Boon P, Vandenberghe S, Vonck K, Marinazzo D. Functional brain connectivity from EEG in epilepsy: Seizure prediction and epileptogenic focus localization. *Prog Neurobiol*. 2014;121:19-35. 10.1016/j.pneurobio.2014.06.004

Wendling F, Ansari-Asl K, Bartolomei F, Senhadji L. From EEG signals to brain connectivity: a model-based evaluation of interdependence measures. *J Neurosci Met.* 2009;183:9-18.

Wilke C, Worrell G, He B. Graph analysis of epileptogenic networks in human partial epilepsy. *Epilepsia.* 2011;*52*(1), 84–93. 10.1111/j.1528-1167.2010.02785.x

Zhang Z, Liao W, Chen H, Mantini D, Ding JR, Xu Q, Wang Z, Yuan C, Chen G, Jiao Q, Lu G. Altered functional-structural coupling of large-scale brain networks in idiopathic generalized epilepsy. *Brain* 2011;134:2912–28.

Patient	Age/Sex	Recording time (hours)	Epilepsy	Side	MRI	Electrodes (left)	Analyzed regions	Seizures	Epilepsy durations (years)	Surgery	Seizure outcome (Engel's class)	Follow up period
1	31/F	24	TLE	R	negative	5 (0)	A, Ha, Hp, TP, Lateral OFC	FS w CA	10	ATL	1A	3 years
2	26/M	24	TLE	R	right amygdala enlargement	7 (0)	A, Ha, Hp, TP, EC, Lateral OFC, TGi	FS w CA/or FS wo CA	11	RFTC	1A	1.5 year
3	31/F	24	TLE	L	negative	7 (7)	A, Ha, Hp, TP, EC, Lateral OFC, PHCp	FS w CA/or FS wo CA/or FS w CA and tonico-clonic bilateral evolution	25	SAH	1B	3 years
4	39/M	24	PCE	L	reduced size of right hippocampus	10 (8)	A, Ha(2), Hp, TP, EC, POC(2), W, AG	FS w CA/or FS wo CA/or FS w CA and tonico-clonic bilateral evolution	38	temporoparietoocciptal resection	1A	5 months
5	25/M	24.5	PCE	R	right hemispheric atrophy	15 (0)	TP, A, Ha, Hp, EC, POC(2), W, AG, Ia, Im, Ip, Lateral OFC, M1	FS w CA/or FS w CA and tonico-clonic bilateral evolution	16	temporoparietoocciptal resection	1B	2 months
6	45/M	24	TLE	L	negative	12 (12)	A, Ha, Hp, TP, EC, iTG, Ia, Ip, TPCp, HS, FB, CGp	FS w CA/or FS w CA and tonico-clonic bilateral evolution	36	RFTC	1A	3 months
7	30/M	23,2	TLE	L	reduced size of left hippocampus	9 (8)	A, Ha(2), Hp, TP, EC, W, PHCp, TOJ	FS w CA/or FS w CA and tonico-clonic bilateral evolution	10	NO	_	_
8	23/M	24	TLE	R	right temporal polar blurring	15 (0)	A, Ha, Hp, TP, EC, PHCp, W, B, TOJ (2), TGs, Lateral OFC (4)	FS w CA/or FS w CA and tonico-clonic bilateral evolution	7	RFTC	1A	3 months
9	40/M	24	TLE	L	left temporal polar blurring	8 (8)	A, Ha, Hp, TP, EC, Lateral OFC, PHCp, TOJ	FS w CA/or FS wo CA/or FS w CA and tonico-clonic bilateral evolution	38	RFTC	3	1.5 year
10	33/F	8,16	TLE	L	left posterior hippocampal lesion	10(9)	A, Ha(2), Hp, TP, EC, Lateral OFC, PHCp, TOJ, Im	FS w CA/or FS w CA and tonico-clonic bilateral evolution	17	ATL	3	2 years

Table 1. Main data of patients included in the study. F = female; M = male; TLE=temporal lobe epilepsy; PCE=posterior cortex epilepsy; R=right; L=left; A=amygdala; Ha=anterior hippocampus; Hp=posterior hippocampus; TP=temporal pole; EC=entorhinal cortex, Lateral OFC=lateral parts of the orbitofrontal cortex; TGi=inferior temporal gyrus; PHCp=posterior parahippocampal cortex; W=Wernicke's area; AG=angular gyrus; Ia=anterior insula; Im=mid insula; Ip=posterior insula; M1=primary motor area; TPCp=posterior temporoparietal cortex; HS=Heschl's area; FB=frontobasal area; CGp=posterior cingulate; TGs=superior temporal gyrus; TOJ=temporal occipital junction; POC=precuneus occipital cortex; B=Broca's area; FS=focal seizure; w=with; wo=without; CA=consciousness alteration; ATL: Anterior temporal lobectomy; RFTC=Radiofrequency thermocoagulation; SAH=Selective amygdalohyppocampectomy; NO=not-operated;

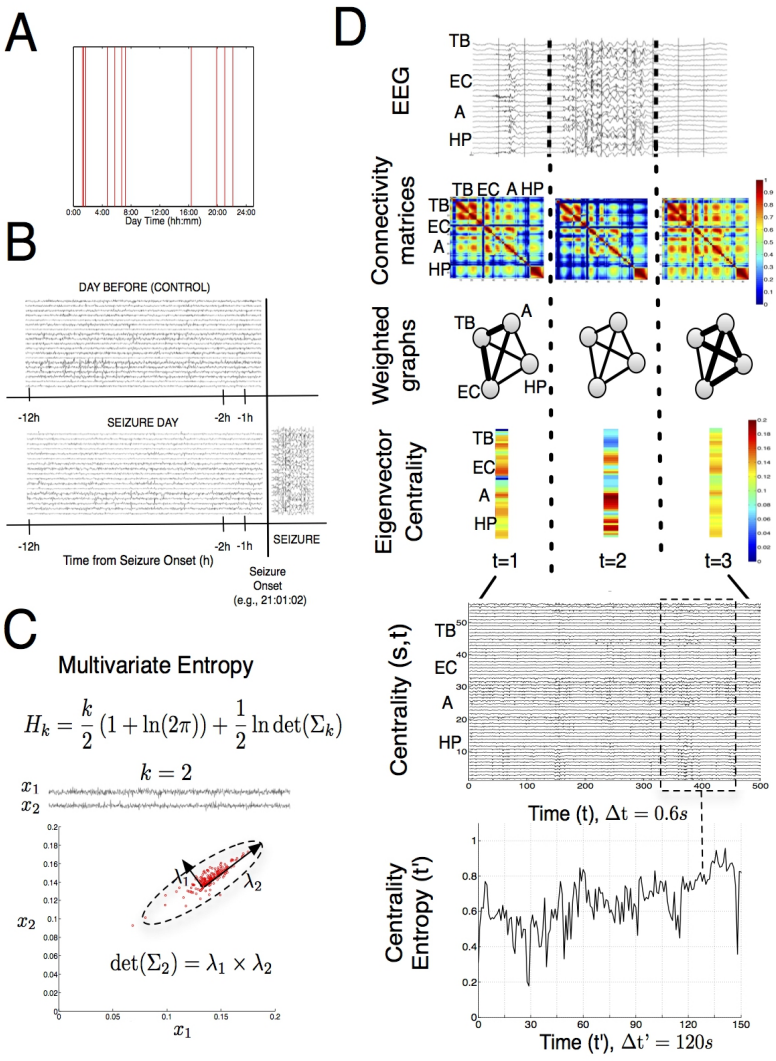

Figure 1. Study paradigm and network dynamics analysis. A: Seizure onset time of the first recorded spontaneous clinical seizure from every patient (n=10). **B:** Schematic representation of the experimental design: for each patient a pre-seizure period of up to 12 hours was matched to the same time period of the previous day that served as a baseline reference (control interictal period). **C:** Multivariate (Gaussian) entropy, showing its dependence on the determinant of the covariance matrix (). Example for a case of two time series in which the determinant of the covariance is shown to shape the joint variability. **D:** Network dynamics analysis: Simultaneous EEG recordings were first divided into consecutive and non-overlapping time windows of 0.6s (Top). Then, functional connectivity matrices were computed using zero-lagged absolute-valued Pearson correlation in each time windows (Middle-top 1). These matrices were modeled as weighted undirected graphs where nodes represented recorded contacts and edges strength represented correlation absolute values (Middle-top 2). The centrality of each contact in every graph was evaluated using the eigenvector centrality leading to a sequence of centrality vectors (Middle-bottom 1). The overall eigenvector centrality sequence was regarded as a set of simultaneous centrality time series (one for each patient recording site over time steps of 0.6s (Middle-bottom 2). Finally, time-dependent centrality entropy values were found for each period of interest by sequentially estimating the multivariate entropy of the centrality time series in non-overlapping and consecutive time windows of 120s (200 samples). The labels TB (Temporal basal area), EC (Entorhinal cortex), A (Amygdala), and HP (Hippocampus) are used as an example to illustrate where the anatomical information was conveyed in each step of the analysis.

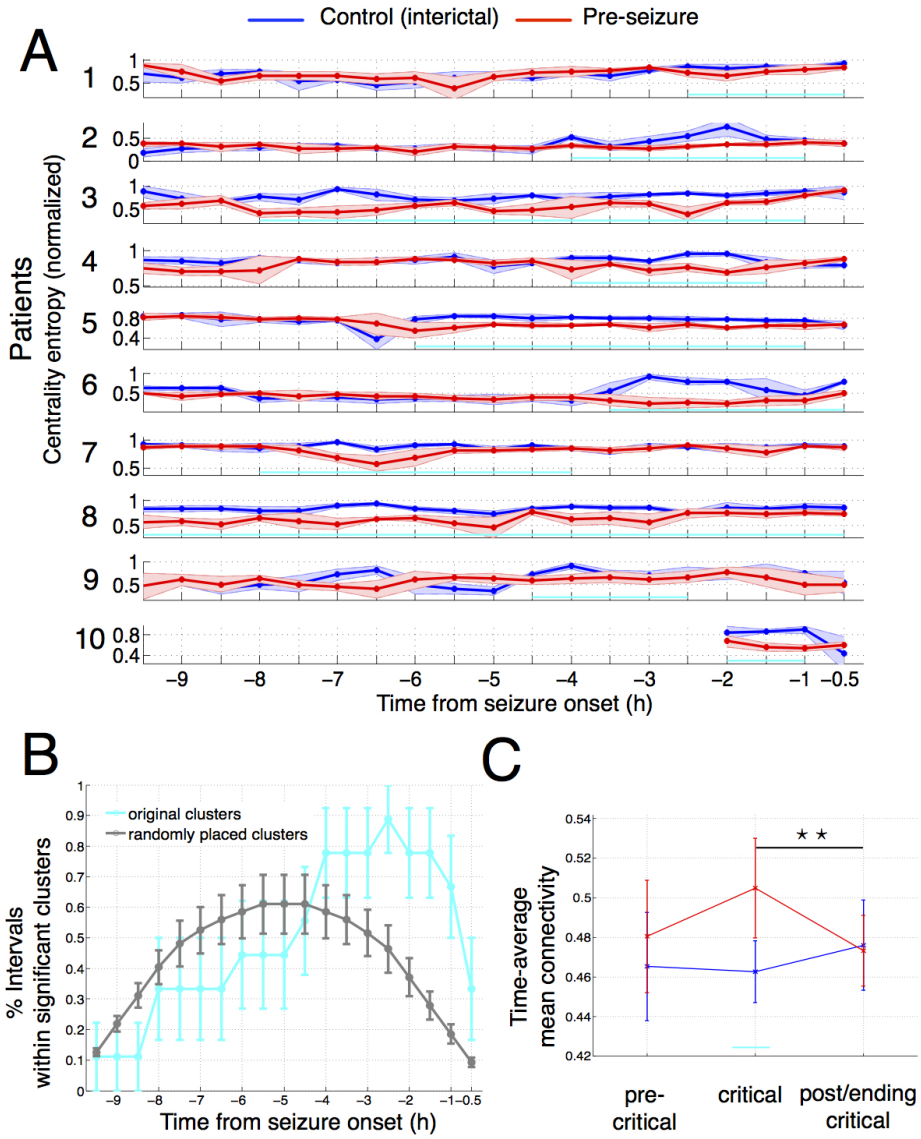

Figure 2. **Time-dependent network state variability decreases near seizure onset during pre-seizure periods**. **A:** Average normalized (to the [0,1] range) centrality entropy for 10 epileptic patients during a pre-seizure period (in red, 9.5 hours before the first seizure) and a control period (in blue, 9.5 hours from the preceding day). Averages were computed over time in non-overlapping windows of 15 entropy samples each (total of 30 min) during both periods. Each entropy sample was computed in a smaller window of 200 subsamples (120s). Curves represent the sequence of centrality entropy mean values and error bars denote ± one standard deviation. In cyan, the sequence of consecutive time steps lying in a significant clusterized difference (randomization test, P<0.01). **B:** Using the first 9 patients, percentage of times that 30-minute intervals lie within a significant cluster. In cyan, significant clusters are located in their original position. In grey, significant clusters are randomly placed along the pre-seizure periods of each patient. Error bars denote SEM (standard error of the mean). **C:** Median (across patients) of the time-average mean functional connectivity along three consecutive sub-periods of interest during pre-seizure and control periods. The first sub-period (pre-critical) comprises intervals prior to the significant cluster, the intermediate sub-period (critical) comprises intervals within the cluster and the last sub-period (post/ending critical) comprises post-cluster intervals. In patients 1, 6 and 8, in which the critical phase was attached to the seizure onset, the last interval was considered to belong to the post/ending critical. Error bars denote SEM (standard error of the mean). Stars denote that there was a significant difference between the critical and the post/ending-critical sub-periods of the pre-seizure period (P<0.01, Wilcoxon test).

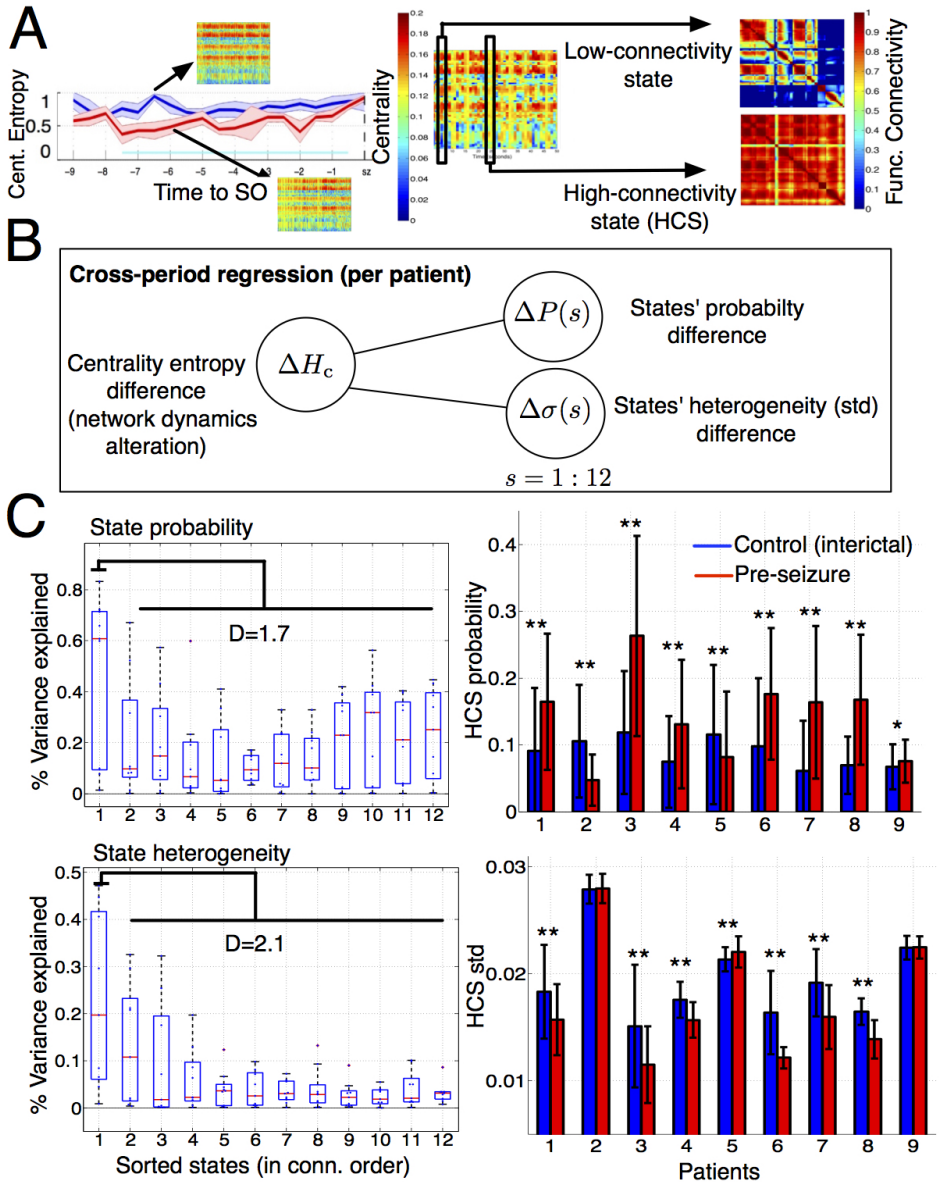

Figure 3: High-connectivity instances influence network dynamics alterations (Patients 1-9) A: Inspection of centrality values around the critical phase (in cyan) suggested a higher presence of homogeneous (yellow strips) values across recording sites during the pre-seizure period (left), which were associated to high-connectivity matrices (HCS, right). Color intensity (blue=lowest, red=highest) represents centrality and connectivity values across recording sites. **B**: Schematic representation (one per patient) of cross-period entropy differences as a function of two families of regressors: changes of (discretized) state probabilities and changes of state homogeneities across recording sites. **C**: Variance explained by each family of regressors (Top, state probabilities; bottom, state homogeneities) in every patient highlights high-connectivity states as a common putative driver of the critical phase. Left: For each patient, discretized states (n=12) were sorted along the horizontal axis in mean connectivity decreasing order. For each sorted state, boxplots show the distribution of the coefficient of determination (%variance explained) of each state across patients. D denotes the effect size (Cohen's D) of the difference between the coefficients of determination of HCS and the remaining states. Right: Cross-period comparison of regressors values associated with high-connectivity state (HCS) during the critical phase between the control and the pre-seizure period. Bars denote the average value of each regressor during the critical phase of the pre-seizure (red) and control periods (blue) per patient. Error bars denote one standard deviation. Upper stars show that the differences in HCS probabilities were significant in all studied patients (* P<0.1, ** P<0.01, paired t-test). All variables in this regression analysis were computed in time windows of 200 time samples (120s).

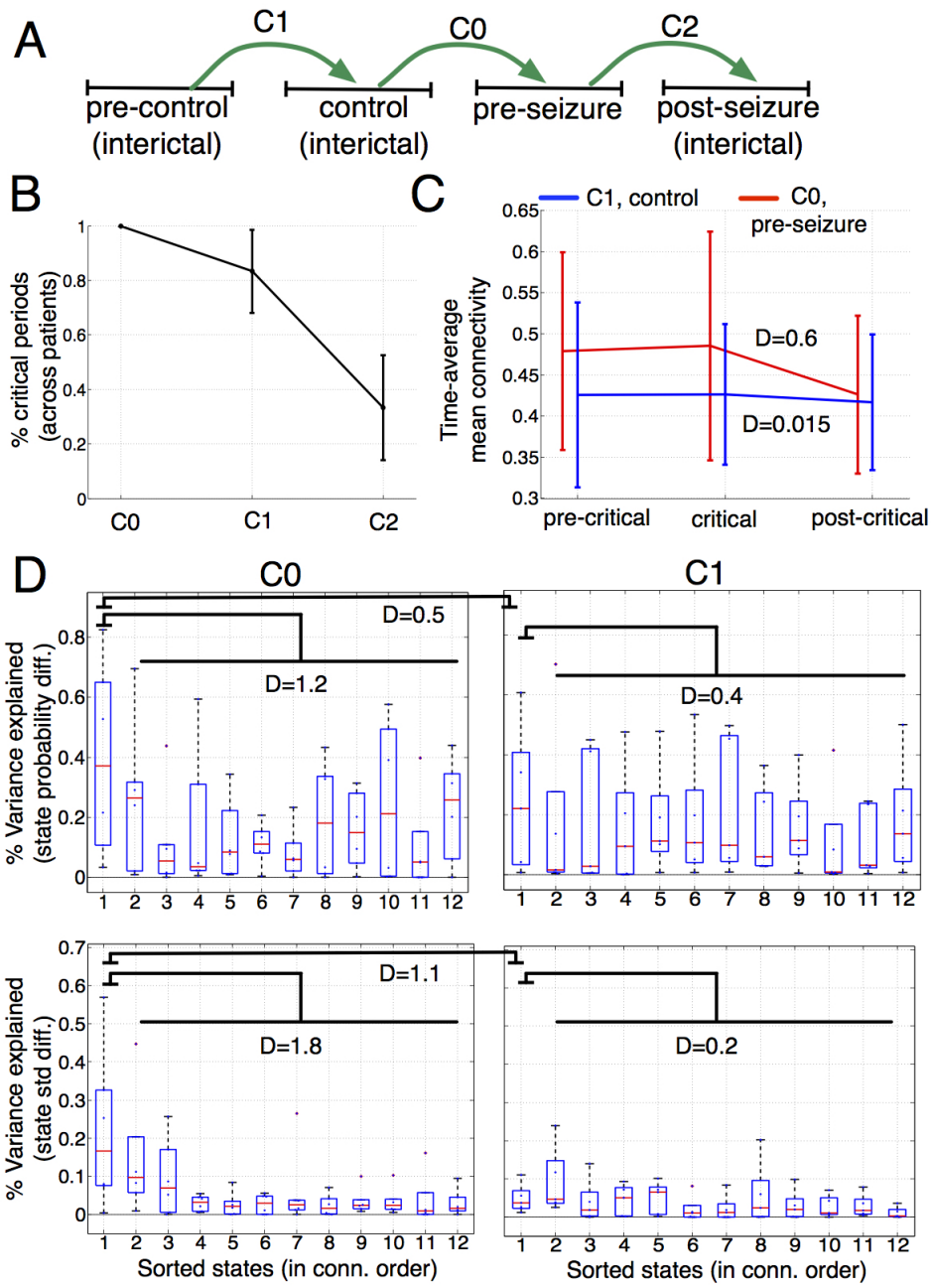

Figure 4: Cross-validation analysis in additional periods (Patients 2-6, and 8) A: Schematic representation of the cross-validation analysis involving Patients 2-6, and 8, and periods of the same lengths (within patient) for the 4 periods. Time-matched periods from 2 days before the seizure (pre-control) and from a varying number of days after the seizure (post-seizure) gave rise to two additional cross-period comparisons (C1 and C2) to the previously analyzed (C0). **B**: Percentage of significant intervals across patients in the cross-period comparisons C0-2 (cluster-based test, P<0.05). **C :** Reproducing the same pre-seizure connectivity curve in Fig. 2C via comparison C0 (in red) and C1 (in blue). D denotes the effect size (Cohen's D) between time-average connectivity values in the critical and post-critical phase (N=6). **D**: Variance explained by each family of regressors of Fig. 3C using the comparison C0 (left) and C1 (right). D denotes the effect size (Cohen's D) of the difference between the coefficients of determination of HCS and the remaining states in each comparison. (bottom), and the effect size of the difference between the coefficients of determination of HCS in comparisons C0 and C1 (top).

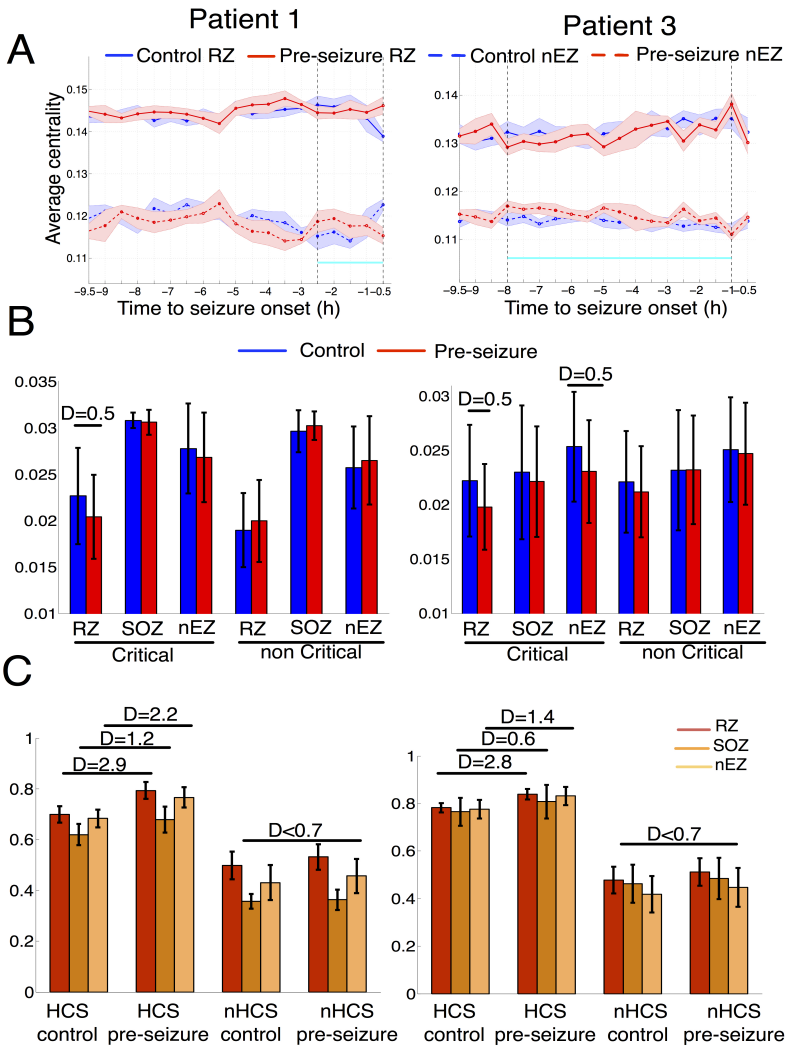

Figure 5: Epileptogenic sites are specifically altered in the critical phase (Patients 1 and 3, Engel 1, follow-up of 3 years, Table 1). In the two patients with best post-surgical outcome after resectomy, recording sites in the resected zone (RZ), seizure onset zone (SOZ) and in none of these regions (nEZ) were independently analyzed (Materials and Methods). **A:** For each patient and period, site-average eigenvector centrality in the RZ, and nEZ averaged within non-overlapping and consecutive time windows of 120s (200 samples) during 9.5 hours prior to seizure onset time. In solid line, average centrality of the RZ. In dashed line, average centrality of the nEZ. Blue and red curves stand for the control and pre-seizure periods respectively. For illustration purposes, curves were averaged within windows of 30 minutes (15 samples per window) to enable direct comparison with the estimated critical phase (highlighted in cyan between two dashed vertical lines). Error bars denote one standard deviation. **B:** Cross-period comparison (control in blue, pre-seizure in red) of sites' centrality variability averaged over RZ, SOZ and nEZ inside (critical, left) and outside (non critical, right) the estimated critical phase (cyan segment in A). Each sample per recording site was computed by performing an average (across pre-ictal and non critical phases) of the centrality's temporal standard deviation measured in non-overlapping and consecutive time windows of 120s (200 samples). Effect sizes larger than 0.5 were reported ("Cohen's d"). **C:** Effect of high-connectivity state into the epileptogenic zone. For each patient, bars showing the site-average connectivity strength RZ, SOZ and nEZ during the high-connectivity clusterized states (HCS, outer left) of both patients and during the remaining states (nHCS, outer right) in control (inner left) and pre-seizure (outer left) periods within the critical phase. Strength samples were computed for each site by performing averages over each set of time instances (HCS and non HCS) during the critical phase. Effect sizes were reported using "Cohen's d". In all subfigures, error bars denote one standard deviation.

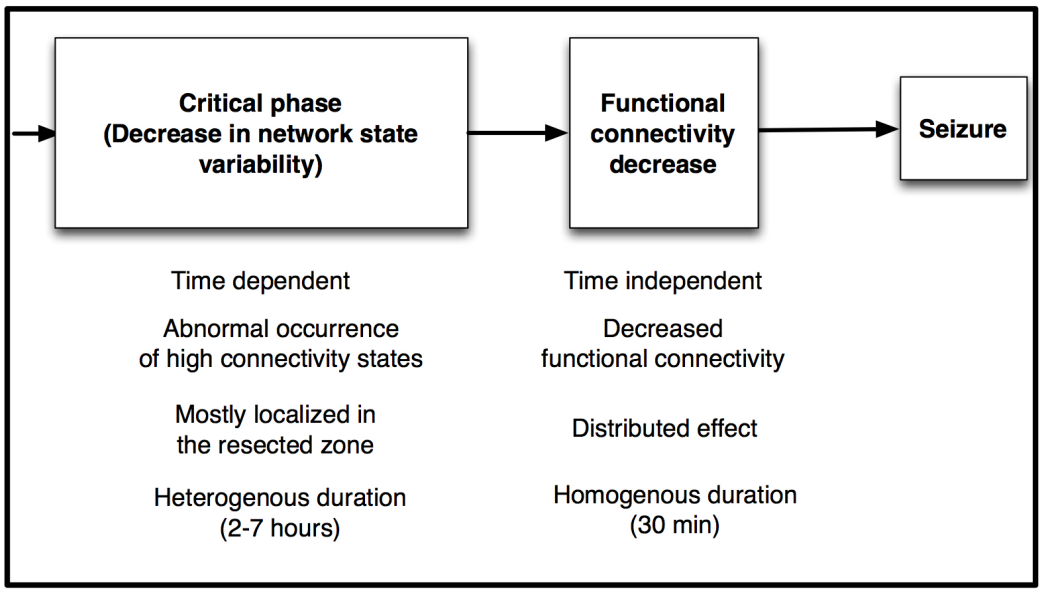

Figure 6: Scheme representing the pre-ictal characterization with two sequential events of different nature and duration: the critical phase and the global functional connectivity decrease.